Research Square

Preprints are preliminary reports that have not undergone peer review.
They should not be considered conclusive, used to inform clinical practice,
or referenced by the media as validated information.

Shape Reserved Stereo Matching with Segment-based Cost Aggregation and Dual-path Refinement

Chih-Shuan Huang
National Cheng Kung University
Ya-Han Huang
National Cheng Kung University College of Bioscience and Biotechnology
Din-Yuen Chan
National Chiayi University
Jar-Ferr Yang (jefyang@mail.ncku.edu.tw)
National Cheng Kung University https://orcid.org/0000-0003-3024-5634

Research

Keywords: stereo matching, depth refinement, simple linear iterative clustering (SLIC), adaptive support weight

Posted Date: June 30th, 2020

DOI: https://doi.org/10.21203/rs.3.rs-16259/v2

License: This work is licensed under a Creative Commons Attribution 4.0 International License.
Read Full License

Version of Record: A version of this preprint was published on September 7th, 2020. See the published version at https://doi.org/10.1186/s13640-020-00525-3.

Abstract

Stereo matching is one of the most important topics in computer vision and aims at generating precise depth maps for various smart applications. The major challenge of stereo matching is to suppress inevitable errors occurring in smooth, occluded and discontinuous regions. In this paper, we propose a robust stereo matching system, which is based on segment-based superpixels, to design adaptive matching computation and dual-path refinement. After the selection of matching costs, we suggest the segment-based adaptive support weights for cost aggregation, instead of color similarity and spatial proximity, to achieve precise depth estimation. Then, the proposed dual-path depth refinement, which refers the texture features in a cross-based support region, corrects the inaccurate disparities to successively refine the depth maps with shape reserving. Specially for left-most and right most regions, the segment-based refinement can greatly improve the mismatched disparity holes. The experimental results show that the proposed system achieves higher accurate depth maps than the conventional stereo matching methods.

Full Text

This preprint is available for download as a PDF.

Tables

Table 1 Image information of Middlebury 2005.

Images	Image Resolutions	Disparity Level
Cones	450 × 375	60
Teddy	450 × 375	60
Tsukuba	384 × 288	16
Venus	434 × 383	20

Table 2 Image information of Middlebury 2014.

Images	Image Resolutions	Disparity Level
Adirondack	718×496	73
ArtL	347×277	64
Jadeplant	659×497	160
Motorcycle	741×497	70
MotorcycleE	741×497	70
Piano	707×481	65
PianoL	707×481	65
Pipes	735×485	75
Playroom	699×476	83
Playtable	680×463	73
PlaytableP	681×462	73
Recycle	720×486	65
Shelves	738×497	60
Teddy	450×375	64
Vintage	722×480	190

Table 3 Error rate (%) of the proposed and other stereo matching algorithms.

Methods		Sun [35]	Hsieh [33]	Lo [31]	E-SM [38]	S-ASW [24]	Proposed
Cones	Non-occ	6.69	5.62	4.44	15.64	7.44	5.59
	All	13.72	13.23	10.96	24.6	13.49	12.06
	Disc	18.70	14.36	10.22	27.22	16.79	13.24
Teddy	Non-occ	10.57	8.75	9.39	20.84	8.73	9.57
	All	17.96	16.23	15.52	28.83	14.78	15.50
	Disc	23.60	26.32	19.16	34.81	23.57	25.08
Tsukuba	Non-occ	6.70	4.26	4.38	5.15	2.59	2.79
	All	8.11	5.18	5.35	7.05	2.89	3.05
	Disc	19.67	17.42	17.12	19.93	13.26	13.93
Venus	Non-occ	1.54	1.98	4.15	5.49	0.48	0.38
	All	2.08	2.43	5.09	7.01	0.68	0.64
	Disc	12.96	6.45	10.71	30.02	4.21	4.88
Average		11.86	9.21	9.23	10.40	9.08	**8.89**

Table 4 Error rate (%) of the proposed and other stereo matching algorithms.

Methods		AdaStereo [39]	tMGM [40]	iResNet [41]	DeepPruner [42]	Proposed
Adirondack	Non-occ	28.1	29.9	25.1	36.9	16.6
ArtL	Non-occ	11.0	11.9	20.2	37.4	30.9
Jadeplant	Non-occ	44.4	28.4	47.9	56.5	21.4
Motorcycle	Non-occ	37.0	16.1	35.6	41.2	11.5
MotorcycleE	Non-occ	37.9	16.1	36.2	41.7	35.5
Piano	Non-occ	39.5	25.8	37.4	37.9	14.2
PianoL	Non-occ	62.2	36.3	59.8	47.4	43.2
Pipes	Non-occ	36.7	14.2	34.5	47.5	16.3
Playroom	Non-occ	49.8	38.5	46.1	52.9	34.4
Playtable	Non-occ	51.4	30.4	40.2	44.9	21.7
PlaytableP	Non-occ	37.6	25.4	25.3	38.6	15.3
Recycle	Non-occ	31.0	31.0	35.0	34.9	10.0
Shelves	Non-occ	63.8	52.7	59.6	52.7	15.5
Teddy	Non-occ	14.5	11.7	15.0	22.9	11.9
Vintage	Non-occ	51.8	52.8	47.7	41.7	30.1
Average		36.6	25.3	35.1	41.2	**21.9**

Figures

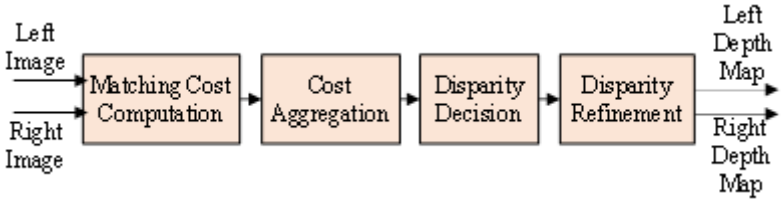

Figure 1

Flow diagram of typical local stereo matching method.

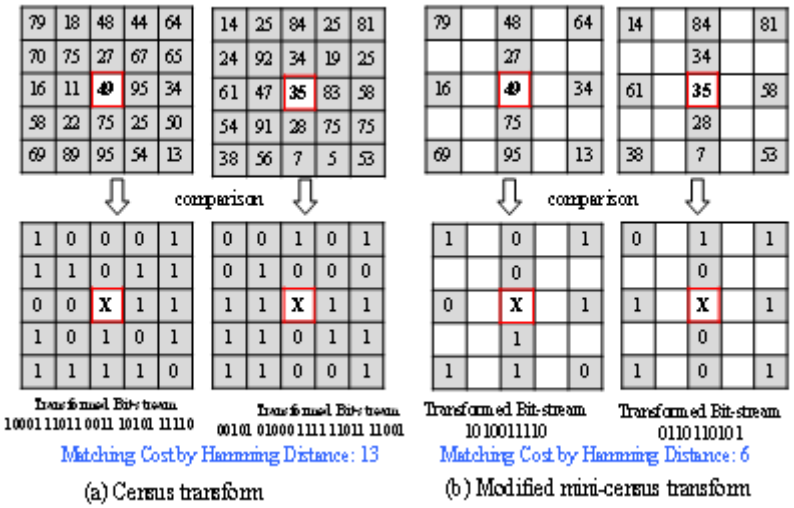

Figure 2

Schematic diagrams of the census and the modified census transforms.

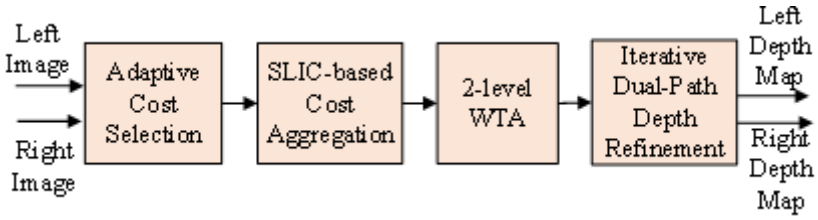

Figure 3

Flowchart of the proposed stereo matching system.

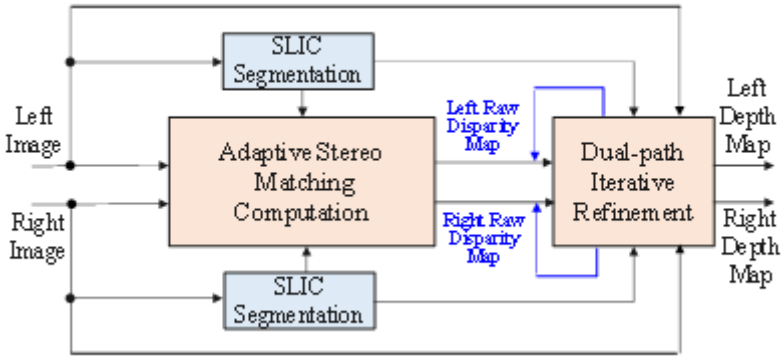

Figure 4

Kernels of the proposed stereo matching system.

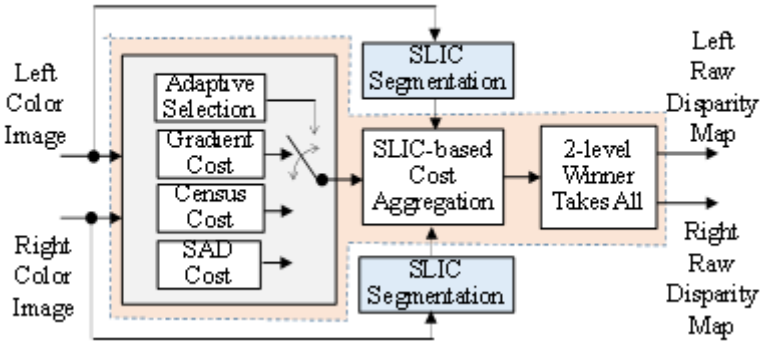

Figure 5

Diagram of the adaptive stereo matching computation unit to estimate left and right raw disparity maps.

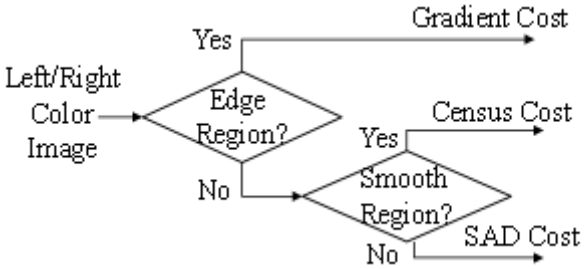

Figure 6

Flow chart of adaptive cost selection strategy

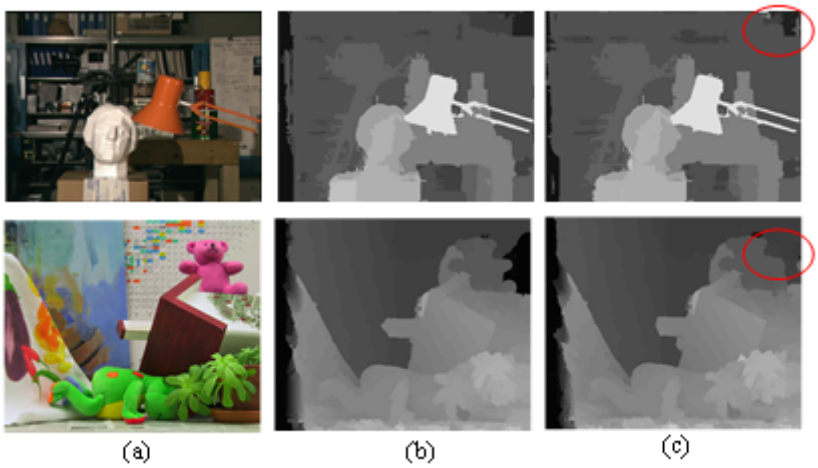

Figure 7

Disparity maps of Tsukuba and Teddy test images achieved by:(a) left color images; (b) direct combined cost; (c) adaptive cost selection.

Figure 8

Results of different levels of the segmented image.

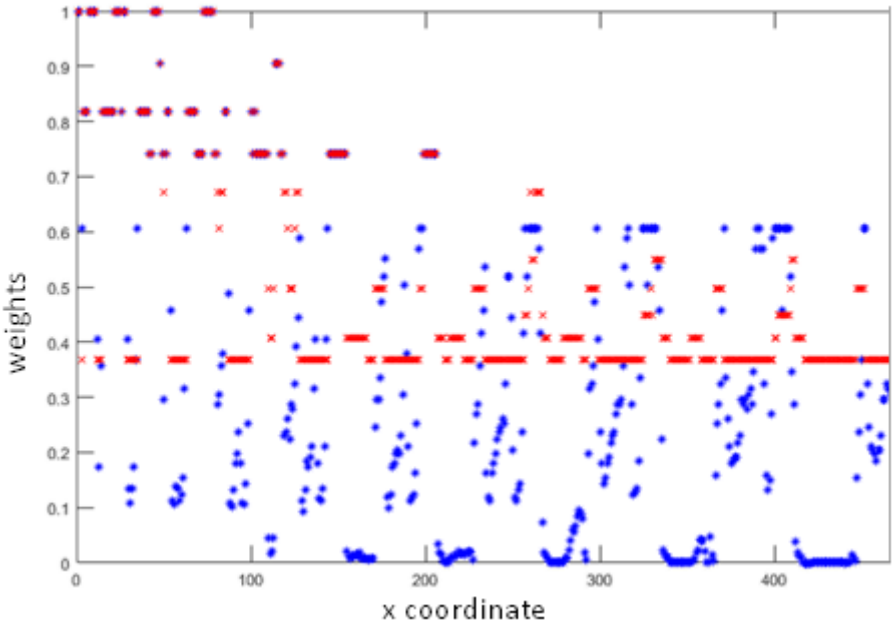

Figure 9

Variations of the SLIC-only and the proposed adaptive aggregation weights.

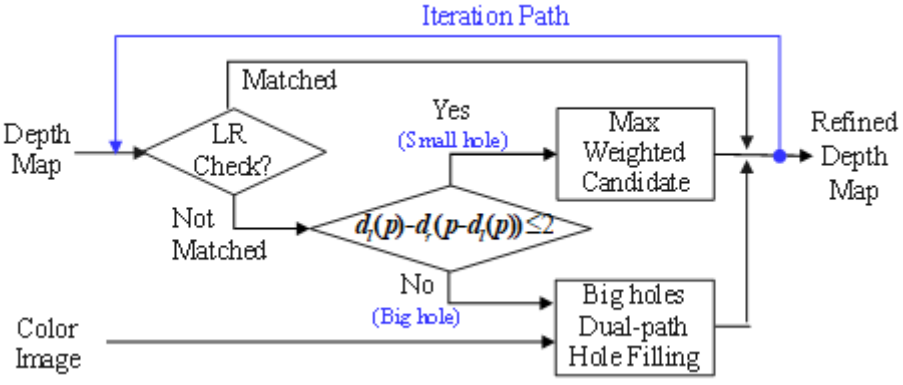

Figure 10

Flow chart of iterative dual-path refinement.

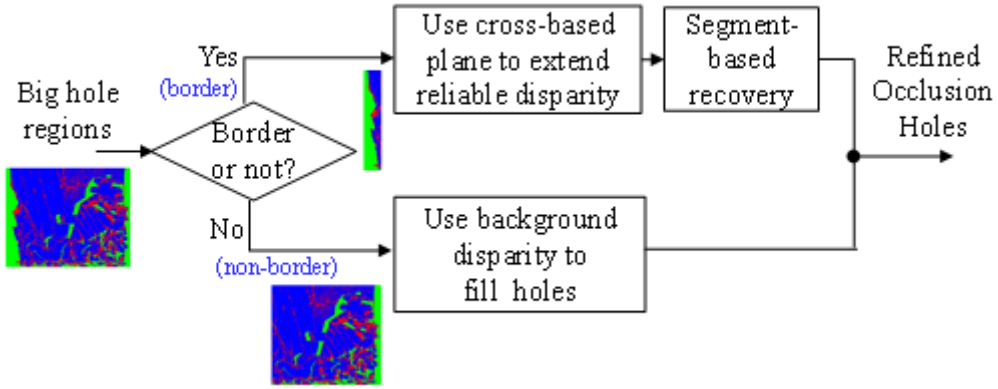

Figure 11

Flow chart of dual-path refinement for big hole regions.

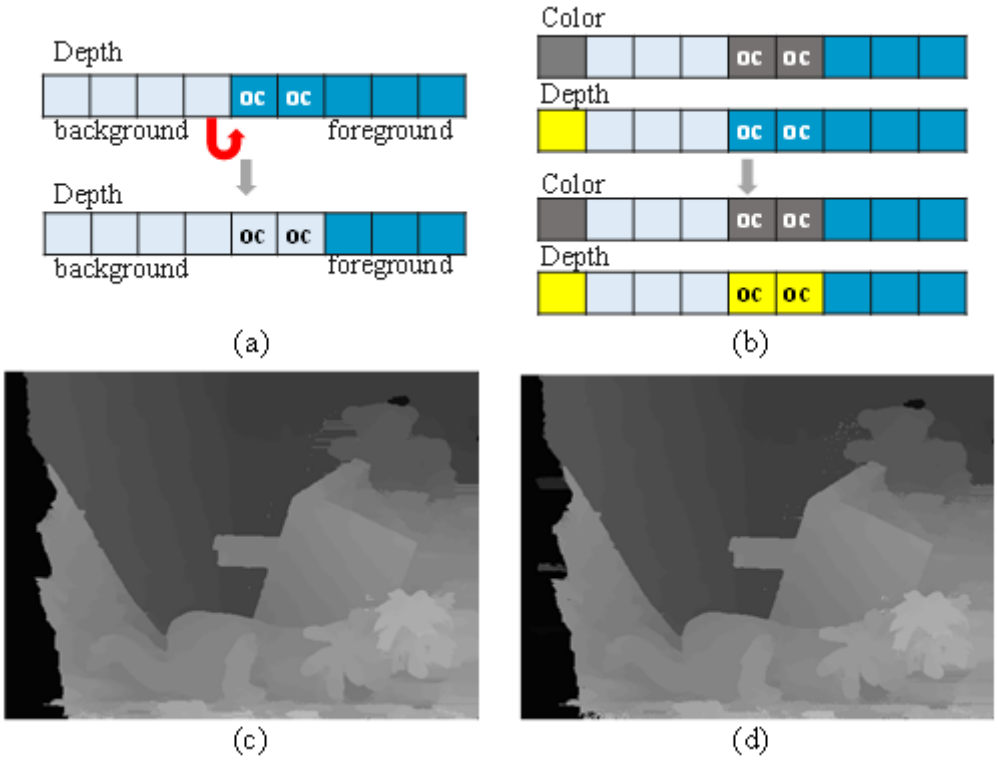

Figure 12

Illustrations and results of the occlusion small-hole background filling methods: (a) regular; (b) matched-color; (c) disparity map by regular; (d) disparity map by matched-color.

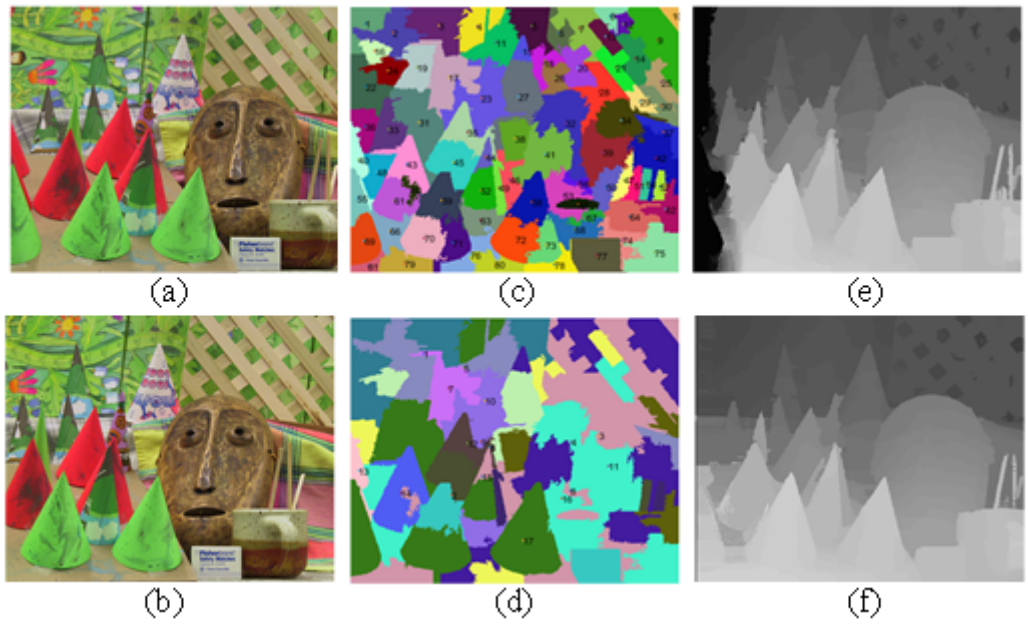

Figure 13

Border disparity segment-based refinement: (a) left color image; (b) right color image; (c) segmented superpixels of left image; (d) merged magapixels of left image; (e) left raw disparity map; (f) left refined disparity map.

Figure 14

Disparity maps for Cones, Teddy, Tsukuba and Venus test images achieved by: (a) raw disparity by the proposed adaptive stereo matching; (b) refined disparity after dual-path refinement.

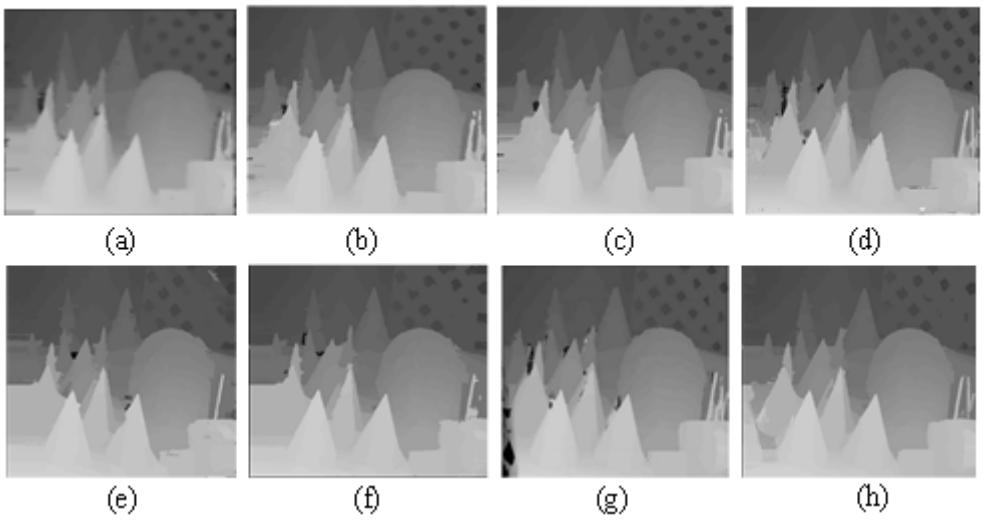

Figure 15

Estimated disparity maps of Cones achieved by (a) Lo [31]; (b) Kuo [32]; (c) Hsieh [33]; (d) Sun [35]; (e) ASW [22]; (f) S-ASW [24]; (g) LF-SM [37]; (h) the proposed method.

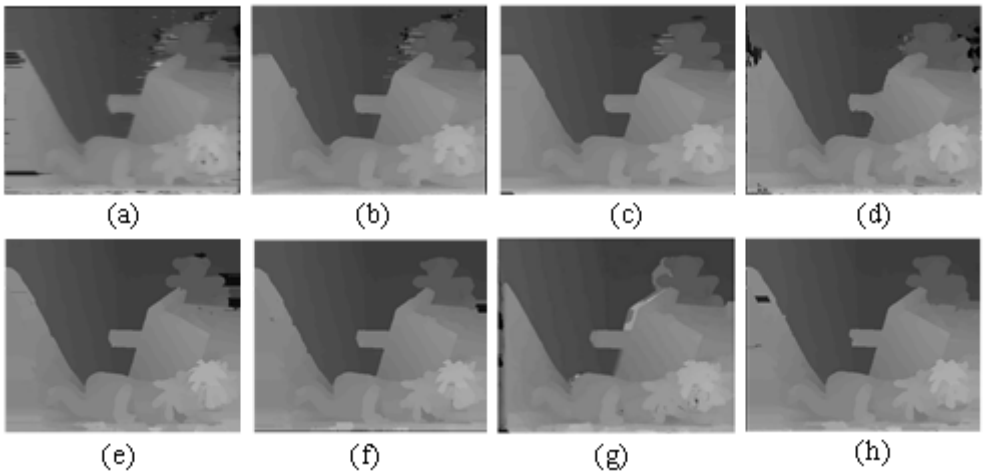

Figure 16

Estimated disparity maps of Teddy achieved by (a) Lo [31]; (b) Kuo [32]; (c) Hsieh [33]; (d) Sun [35]; (e) ASW [22]; (f) S-ASW [24] ; (g) LF-SM [37]; (h) the proposed methods.

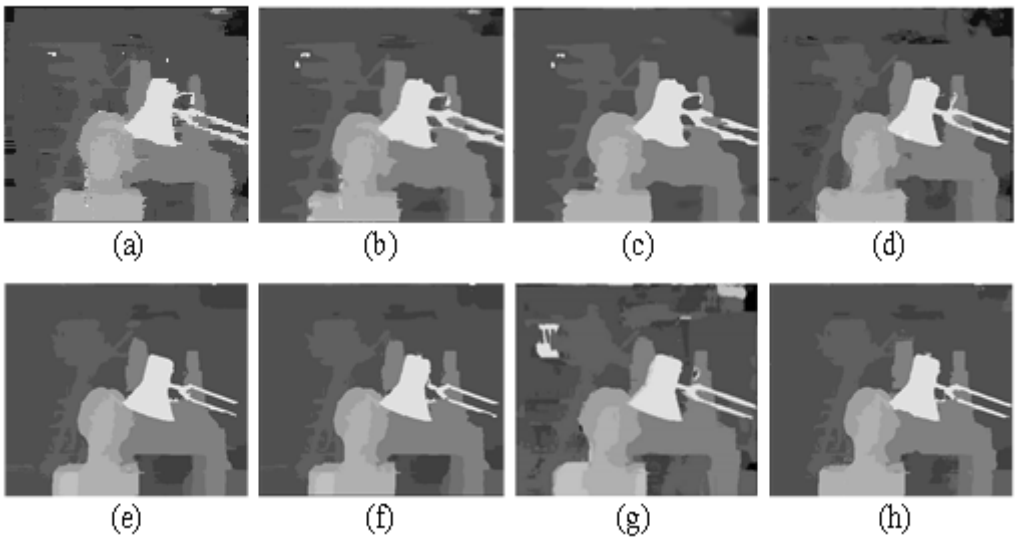

Figure 17

Estimated disparity maps of Tsukuba achieved by (a) Lo [31]; (b) Kuo [32]; (c) Hsieh [33]; (d) Sun [35]; (e) ASW [22]; (f) S-ASW [24] ; (g) LF-SM [37]; (h) the proposed methods.

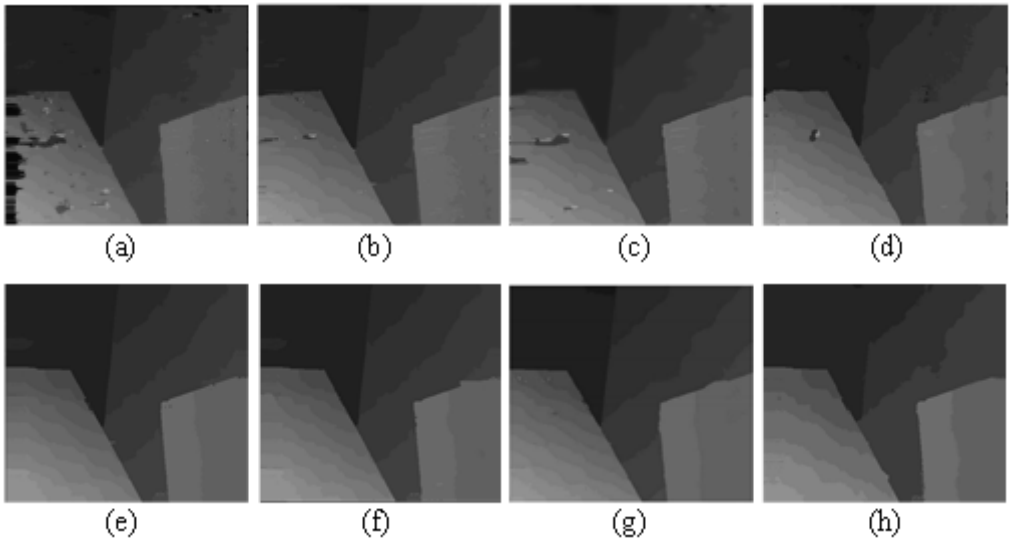

Figure 18

Estimated disparity maps of Venus achieved by (a) Lo [31]; (b) Kuo [32]; (c) Hsieh [33]; (d) Sun [35]; (e) ASW [22]; (f) S-ASW [24] ; (g) LF-SM [37]; (h) the proposed methods.